Appendix D:

Evidence for the Predominance of Mid-Tropospheric Aerosols as Subtropical Anvil Cloud Nuclei*

27. R. Bessinger, P. Akwara, "Trends in Sexual and Fertility-Related Behavior: Cameroon, Kenya, Uganda, Zambia, and Thailand" (The Measure Evaluation Project, United States Agency for International Development, Washington, DC, 2003) (www.cpc.unc.edu/measure/publications/pdf/sr-03-21b.pdf).
28. "South African national HIV prevalence, behavioral risk, and mass media household survey," (Nelson Mandela Children's Fund and the Human Sciences Research Council, Capetown, South Africa, 2002).
29. L. McKusick, W. Horstman, T. Coates, *Am. J. Public Health* **75**, 493 (1985).
30. K. Witte, M. Allen, *Health Educ. Behav.* **27**, 608 (2000).
31. UNAIDS, "A measure of success in Uganda" (UNAIDS, Geneva, Switzerland, 1998).
32. UNAIDS, "Trends in HIV incidence and prevalence: natural course of the epidemic or results of behavior change?" (UNAIDS, Geneva, Switzerland, 1999).
33. E. Korenromp *et al*., *AIDS* **16**, 2209 (2002).
34. R. Stoneburner, L. Lessner, J. Fordyce, P. Bevier, M. Chiasson, *Am. J. Epidemiol.* **138**, 1093 (1993).
35. A. J. Nunn *et al*., *Br. Med. J.* **315**, 767 (1997).
36. Peter Mugyenyi, personal communication.
37. Kamali *et al.*, *Lancet* **361**, 645 (2003).
38. R. Moodie *et al*., "An evaluation study of Uganda's AIDS control programmes' information, education, and communication activities" (WHO/Uganda Ministry of Health, 1991).
39. G. Kwesigabo *et al.*, *J. Acquir. Immune Defic. Syndr.* **23**, 410 (2000).
40. R. L. Stoneburner, D. Low-Beer, *Int. J. Epidemiol.*, in press.
41. D. Tarantola, B. Schwartlander, *AIDS* **11,** S5 (1997).
42. M. J. Wawer *et al*., *AIDS* **11**, 1023 (1997).
43. R. Stoneburner, M. Carballo, R. Bernstein, T. Saidel, *AIDS* **12**, 226 (1998).
44. G. Rose, *The Strategy of Preventive Medicine* (Oxford Medical Publications, Oxford, 1992).
45. "ANC sentinel surveillance of HIV/Syphillis Trends in Zambia, 1994–2002" (Central Board of Health, Lusaka, Zambia, 2004).
46. The authors thank E. C. Green for insight, advice, and support and I. Katz for support in analysis. This work was supported in part by funding from Family Health International contract no. HRN-5972-Q-00-4002-00 (1996–1997) and USAID grant no. Afr.-G-009770008-00 (1998–2000). The opinions expressed in this article are those of the authors and in no way reflect policy of the United States government, the United States Agency for International Development, or the University of Cambridge.

Supporting Online Material

www.sciencemag.org/cgi/content/full/304/5671/714/DC1
Materials and Methods
SOM Text
Figs. S1 and S2
Tables S1 to S4
References

31 October 2003; accepted 30 March 2004

Evidence for the Predominance of Mid-Tropospheric Aerosols as Subtropical Anvil Cloud Nuclei

Ann M. Fridlind,[1]* Andrew S. Ackerman,[1] Eric J. Jensen,[1] Andrew J. Heymsfield,[2] Michael R. Poellot,[3] David E. Stevens,[4] Donghai Wang,[5] Larry M. Miloshevich,[2] Darrel Baumgardner,[6] R. Paul Lawson,[7] James C. Wilson,[8] Richard C. Flagan,[9] John H. Seinfeld,[9] Haflidi H. Jonsson,[10] Timothy M. VanReken,[9] Varuntida Varutbangkul,[9] Tracey A. Rissman[9]

NASA's recent Cirrus Regional Study of Tropical Anvils and Cirrus Layers–Florida Area Cirrus Experiment focused on anvil cirrus clouds, an important but poorly understood element of our climate system. The data obtained included the first comprehensive measurements of aerosols and cloud particles throughout the atmospheric column during the evolution of multiple deep convective storm systems. Coupling these new measurements with detailed cloud simulations that resolve the size distributions of aerosols and cloud particles, we found several lines of evidence indicating that most anvil crystals form on mid-tropospheric rather than boundary-layer aerosols. This result defies conventional wisdom and suggests that distant pollution sources may have a greater effect on anvil clouds than do local sources.

It is well understood that cloud drops form on existing atmospheric aerosols, such as sulfuric acid particles and dust. Thus, changes in aerosol number can lead to changes in drop number during cloud formation. Complex subsequent effects on cloud microphysical development vary depending on cloud type and environmental conditions (*1*). The overall impact of increasing anthropogenic aerosols on low clouds such as stratocumulus may be great, generally resulting in smaller, more numerous drops and leading to brighter, longer-lived clouds that reflect more sunlight (*2*, *3*). Because stratocumulus clouds persistently cover large global areas, it has been recognized that this aerosol-induced cooling effect partially offsets the warming effect of accumulating greenhouse gas concentrations (*4*).

Whereas low clouds such as stratocumulus alter the global solar radiative budget with little influence on the infrared budget, high clouds such as cirrus reduce both solar incoming and infrared outgoing radiative fluxes by comparable amounts. Whether the overall impact is warming or cooling depends in a sensitive manner on cloud optical depth and ice crystal effective radius (*5*), among other factors. Although cirrus clouds have a much lesser influence on the net radiative budget per unit area than stratocumulus, the area covered by tropical anvil clouds may respond strongly to increasing sea surface temperatures, thereby playing a major role in global climate sensitivity (*6–8*). However, the properties and evolution of anvil cirrus clouds remain poorly understood and weakly constrained in models (*9*). Recent observations also suggest that tropical cloud coverage may be rapidly changing in a manner not captured by current general circulation model simulations (*10*), which serves as further motivation to seek a better understanding of anvil-forming cumulonimbus clouds.

The Cirrus Regional Study of Tropical Anvils and Cirrus Layers–Florida Area Cirrus Experiment (CRYSTAL-FACE) was coordinated by NASA with the primary goal of fully characterizing subtropical cumulonimbus anvil formation and evolution. The experiment took place throughout July 2002 over southern Florida, where simultaneous measurements were made from six aircraft and three ground stations, as well as satellite platforms, over the lifetimes of many storm systems. The data gathered included simultaneous measurements of the number and size distribution of aerosols and cloud particles throughout the full depth of developing cumulonimbus columns. Whereas a handful of previous modeling studies and data analyses have addressed the potential impact of boundary-layer aerosol loading on the microphysical properties of clouds associated with deep convection (*11–14*), here we incorporate these extensive new measurements into a detailed three-dimensional (3D) modeling analysis with appropriate vertical variation of the aerosol field.

[1]National Aeronautics and Space Administration (NASA) Ames Research Center, Moffett Field, CA 94035, USA. [2]National Center for Atmospheric Research, Boulder, CO 80307, USA. [3]Department of Atmospheric Sciences, University of North Dakota, Grand Forks, ND 58202, USA. [4]Lawrence Livermore National Laboratory, Livermore, CA 94552, USA. [5]Center for Atmospheric Sciences, Hampton University and NASA Langley Research Center, Hampton, VA 23681, USA. [6]Centro de Ciencias de la Atmosfera, Universidad Nacional Autonoma de Mexico, Mexico City, DF 04510, Mexico. [7]Stratton Park Engineering Company, Inc., Boulder, CO 80301, USA. [8]Department of Engineering, University of Denver, Denver, CO 80208, USA. [9]Division of Chemistry and Chemical Engineering, California Institute of Technology, Pasadena, CA 91125, USA. [10]Center for Interdisciplinary Remotely-Piloted Aircraft Studies, Marina, CA 93933, USA.

*To whom correspondence should be addressed. E-mail: ann.fridlind@nasa.gov

An unexpected result of this study is our finding that the fundamental source of the nuclei on which most anvil crystals initially form is the mid-troposphere at 6 to 10 km rather than the planetary boundary layer near the Earth's surface (*13*). Several lines of evidence for this conclusion emanate from a case study of the highest strength updraft (>20 m s^{-1}) that was penetrated directly by aircraft during the CRYSTAL-FACE campaign on 18 July. Because most cloud particles are formed in high-strength updraft cores, where supersaturations reach peak values (*15*), these measurements provide a unique window into the microphysical environment governing the injection of cloud particles into anvil cirrus clouds. Although CRYSTAL-FACE conditions did not include deep convection in the presence of heavy smoke or active fires (*14*), they were representative of subtropical continental deep convection.

On 18 July, the University of North Dakota Citation aircraft measured aerosols and cloud particles at 7 to 12 km along the developing sea breeze fronts and penetrated the high-strength updraft east of Lake Okeechobee at an altitude of about 10 km (Fig. 1). Meanwhile, the Center for Interdisciplinary Remotely-Piloted Aircraft Studies (CIRPAS) Twin Otter aircraft measured aerosols and cloud particles between the surface and 4 km over the southwest Florida peninsula. NASA's WB-57 aircraft, which generally measured aerosols and cloud particles at 12 to 16 km, did not operate on 18 July, but we were able to use WB-57 aerosol and cloud observations collected under similar conditions on other days to complement this case study. We thus incorporated observations from all three aircraft making in situ measurements during CRYSTAL-FACE (*16*).

To simulate the development of high-strength updrafts similar to the one observed, we used 3D large-eddy simulations with size-resolved microphysics (*16*–*19*). We initialized the model domain with a meteorological profile derived from local rawinsonde measurements (*16*) and an aerosol profile (Table 1) derived from aircraft measurements (*16*). Surface heat and moisture fluxes were assimilated from mesoscale weather model predictions for 18 July (*16*, *20*) at the location of observed convection. The model transports aerosols, liquid drops, and ice particles, accounting for activation, condensational growth, evaporation, sedimentation, and melting (*21*); gravitational collection (*21*–*23*); spontaneous and collision-induced drop breakup (*22*, *24*); homogeneous and heterogeneous freezing of aerosols and drops (*21*, *25*); and Hallett-Mossop rime splintering (*21*). Simulations exhibited chaotic generation of mature high-strength updrafts throughout the last 2 hours of each 3-hour simulation. We then compared simulated cloud particle properties in updrafts of similar strength with measurements made in the updraft on 18 July and in typical thick anvil clouds on 21 July.

First comparing simulations with measurements made in the updraft core on 18 July, we found that it was necessary to include tropospheric aerosols above 6 km in order to accurately simulate the large number of cloud particles observed (Fig. 2). Aerosols below 2 km, which well exceeds the typical 1-km boundary-layer height, were insufficient to account for the observed numbers of cloud particles. Aerosols below 6 km were also insufficient, but when all aerosols up to the updraft-penetration altitude of 10 km were included in the simulation, the number of cloud particles as a function of vertical wind speed closely matched the observations. Furthermore, in both simulations and measurements, peak particle numbers were not

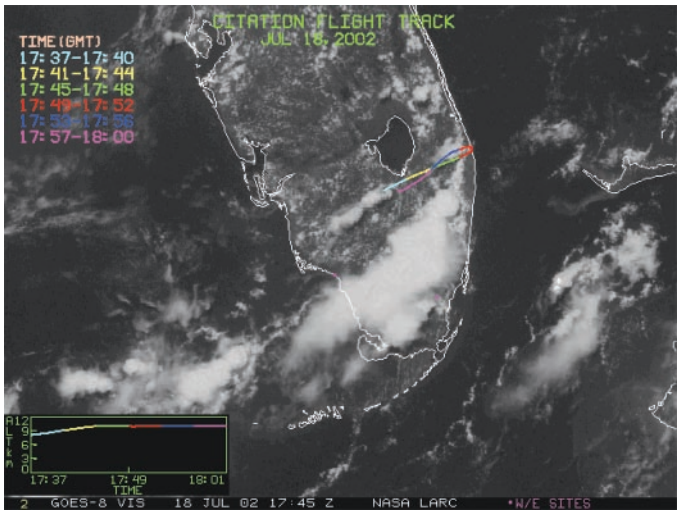

Fig. 1. Flight track of the Citation aircraft through the developing updraft core on 18 July, directly east of Lake Okeechobee. The experiment-wide peak updraft speed of about 23 m s^{-1} was measured at 17:49:10 UTC, 4 min after the underlying satellite image was taken. [Figure courtesy of Patrick Minnis and Louis Nguyen, NASA Langley Research Center]

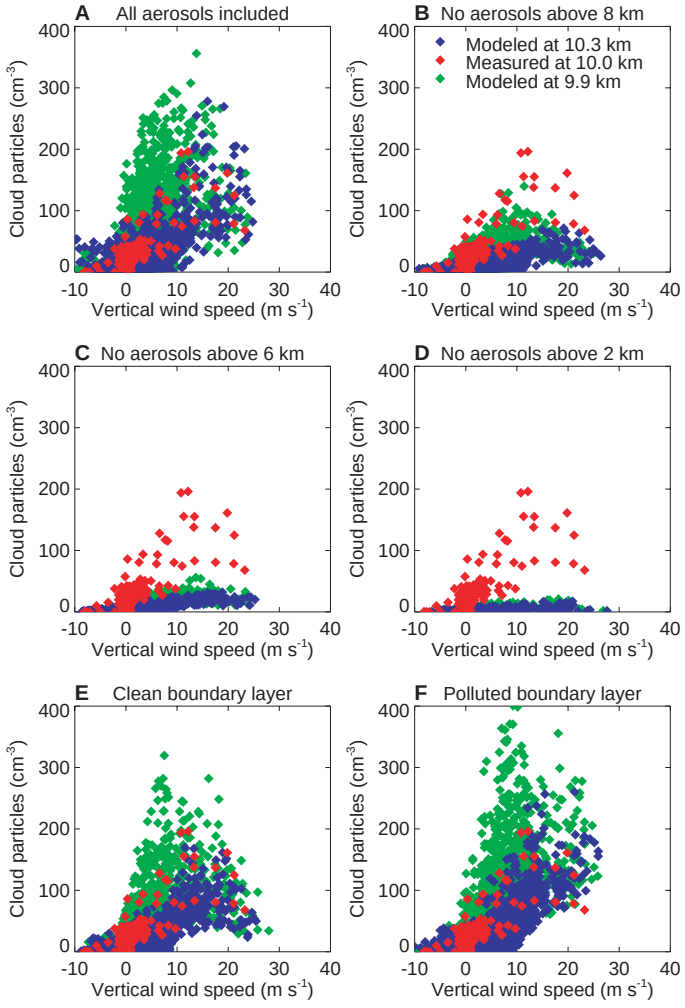

Fig. 2. Cloud particle number versus vertical wind speed measured near 10-km altitude in the updraft core (red) and simulated in the nearest layers above and below 10 km (blue and green, respectively) when simulated peak vertical wind speeds are similar to those observed. Model results show closest agreement with observations when all aerosols are included in the simulation (**A**). Agreement degrades when free tropospheric aerosols are excluded above 8 km (**B**), 6 km (**C**), and 2 km (**D**) and is less sensitive to replacing moderate aerosol concentrations of 1800 per cm^3 in the boundary layer with clean marine aerosols of 400 per cm^3 (**E**) or polluted aerosols of 6500 per cm^3 (**F**). See Table 1 for aerosol number size distribution parameters.

found at peak updraft speeds, where peak supersaturations are located, but instead were found at intermediate updraft speeds (Fig. 2A). This pattern, coupled with the importance of entrained mid-tropospheric aerosols to reproducing the observed cloud particle number concentrations, suggests that the highest particle numbers are found in an entraining region of the updraft core. In the entrainment region, turbulent mixing laterally brings in mid-tropospheric aerosols, which are exposed to higher supersaturations, activated, and then carried aloft.

A second line of evidence derives from a closer examination of the measured variation of cloud particle size distribution during the updraft traversal, which was flown horizontally from downwind to upwind. When we chose a similar path through a simulated updraft core and compared it with these measurements, both measurements and simulation results showed that the peak number was reached upwind of the peak vertical wind speed as the core was traversed (Fig. 3, A and B). This region in which particle numbers reached their peak values was also characterized by a mixture of source air (Fig. 3, C and D), indicative of substantial entrainment. In both simulations and observations, we also found that the additional cloud particles in this upwind entraining region were much smaller than those in the heart of the core (Fig. 3, E and F), which is the pattern that would be expected in the case of activation on recently entrained free tropospheric aerosols.

Finally, we considered whether simulated cloud particle number and size matched observations in the upper anvil cloud, where high-strength updraft cores detrain. Although the upper-level anvil cloud was not sampled on 18 July, anvil clouds from similar small cumulonimbus systems were sampled on 11, 16, 19, 21, and 28 July. Using observations in a typical thick anvil cloud between 12 and 14 km on 21 July as an example (other days appeared similar), we found that the measurements consistently indicated peak crystal number concentrations in the diameter range of 20 to 30 μm. Model simulations on 18 July reproduced this peak accurately and consistently when aerosols were included throughout the atmospheric column, but the peak shifted to 50 to 60 μm when aerosols above 6 km were excluded, and it shifted to even larger sizes when aerosols above 2 km were excluded (Fig. 4). These comparisons in the upper-level anvil clouds support our analysis of the updraft measurements, providing a third line of evidence for the importance of mid-tropospheric aerosols. Because peak size was negligibly affected when aerosols above 10 km were excluded, those did not appear to be an important source of anvil nuclei. We estimate that the aerosols entrained between 6 and 10 km account for about two-thirds of the anvil nuclei (Fig. 4, compare B to D). We obtained similar results in simulations of convective events on other days during CRYSTAL-FACE, despite varying updraft strength and thermodynamic conditions.

It is initially surprising to find that mid-tropospheric aerosols determine fundamental anvil properties, because deep convection updraft cores are generally assumed to be relatively undiluted parcels that travel from cloud base to cloud anvil with little entrainment

Table 1. Aerosol profile number and log-normal size distribution parameters.

Elevation (km)	Number (cm^{-3})	Mode diameter (μm)	Standard deviation
	Baseline		
15*	100	0.025	1.6
10†	3000	0.025	1.6
5‡	1200	0.025	1.6
2§	1200	0.05	2.5
<1‖	1800	0.11	1.9
	Clean		
<1¶	400		
	275	0.035	1.5
	125	0.11	1.4
	Polluted		
<1#	6500		
	3000	0.03	1.5
	3500	0.12	1.8

*Because no WB-57 aircraft measurements are available for 18 July, typical number and size distribution parameters for the uppermost troposphere are derived from measurements made on 19 July. †The number concentration of aerosols at 10 km is set to the number measured by the Citation aircraft upon entering the updraft-containing cloud. Because no size distribution measurements are available for the Citation, typical size distribution parameters measured by the WB-57 on 19 July are assumed. ‡The number concentration of aerosols at 5 km is set to the typical number measured by the Citation on 18 July at that elevation. §The number concentration of aerosols at 2 km is set to the typical number measured by both Citation and Twin Otter aircraft on 18 July at that elevation. Size distribution parameters are derived from Twin Otter measurements made in the vicinity of that number concentration and elevation on 18 July. ‖All 18 July Twin Otter measurements were made over the southwest peninsula, downwind of continental and pollution sources, whereas the high-strength updraft formed at the east coast in onshore winds. Baseline number concentration and size distribution are therefore derived from the cleanest boundary-layer aerosols sampled by the Twin Otter on 18 July. ¶Clean sensitivity test parameters were derived from Twin Otter measurements of marine boundary-layer aerosols sampled on 25 July, which were markedly bimodal and are therefore represented as the sum of the two modes listed. No such clean conditions were encountered on 18 July. #Polluted sensitivity test parameters were derived from measurements of boundary-layer aerosols sampled on 18 July, which were also strongly bimodal.

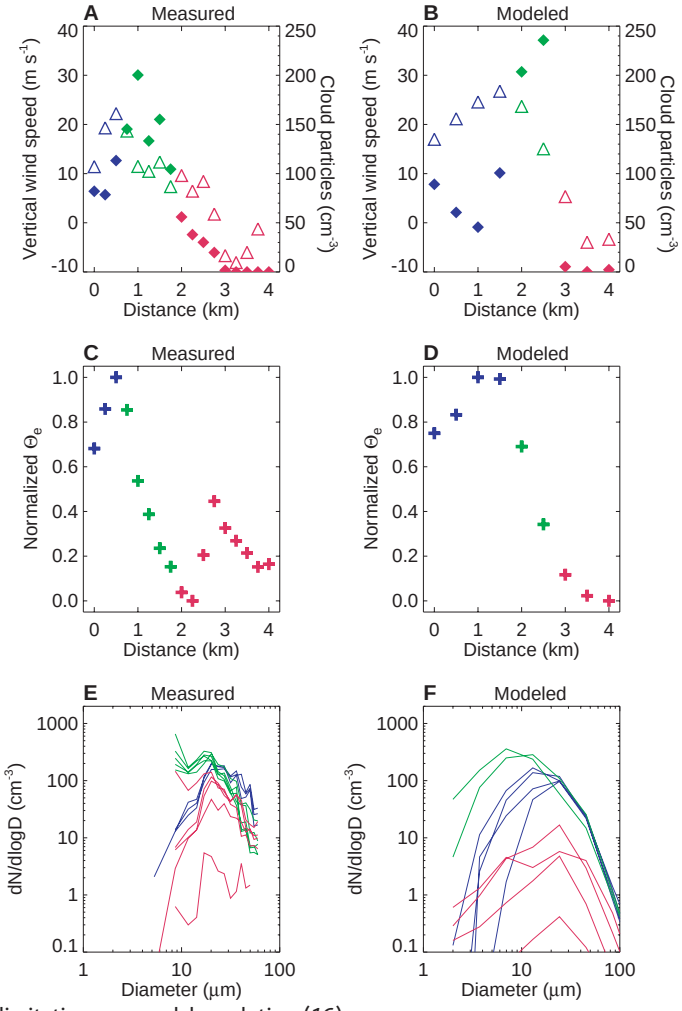

Fig. 3. Comparison of 2-s average measurements across the updraft (**A**) with results along a 4-km path through an updraft of similar strength in the baseline simulation (**B**). Updraft strength (triangles) and cloud particle number concentration (diamonds) are denoted by color in three regions: downwind in the core (blue), within the entrainment region (green), and upwind of the core (red). Equivalent potential temperatures, Θ_e, normalized by their respective measured and simulated ranges, demonstrate that the green points occupy an entrainment region of both the measured updraft (**C**) and the simulated updraft (**D**). Cloud particle size distributions, $dN/d\log D$, show that the entrainment region is characterized by increased numbers of the smallest particles in both measurements (**E**) and simulation results (**F**). The simulated core is generally wider and more uniform than the observed core at least in part because of limitations on model resolution (*16*).

(*13*). However, this assumption has recently been challenged by Zipser (*26*), who makes a distinction between relatively undiluted, high velocity, mid-latitude supercell updrafts and highly diluted, lower velocity, tropical marine updrafts. The updrafts observed during CRYSTAL-FACE appear to lie along this continuum, with intermediate vertical wind speed and dilution. Analysis of laboratory thermals indicates that entrainment scales inversely with updraft diameter (*15*), and when the toroidal rotation of rising updrafts is considered, also provides the rule of thumb that an updraft is turned "inside out" once over a vertical distance of about 1.5 diameters (*27*). Whereas the updraft cores of mid-latitude supercells may be 18 km in diameter (*28*), corresponding to less than a full toroidal rotation during ascent to the tropopause, the Florida updraft observed on 18 July exhibited an updraft diameter of less than 5 km, corresponding to about two such rotations. These order-of-magnitude estimates support the role of mid-tropospheric entrainment.

There are important implications of our finding that anvil crystal number and size are determined by the entrainment of mid-tropospheric aerosols. Crystal size itself is a leading factor controlling cirrus radiative properties, with smaller crystals corresponding to higher cloud albedo (*5*). Owing to the apparently widespread presence of small anvil crystals in recent measurements, Garrett *et al*. (*29*) argue that there may be a need for substantial corrections to parameterizations of cirrus clouds in global climate models. It has also been suggested that the size of anvil ice crystals may control relative humidity near the tropopause and, by extension, moisture transport into the lower stratosphere (*30*, *31*). By attributing anvil crystal formation to entrained mid-tropospheric aerosols (Fig. 4), we also provide a new explanation for the generation of copious small crystals that have been reported at anvil tops (*32*). The source of such crystals has been a puzzle, and they have been previously attributed to aerosol activation either at the cloud top (*32*) or at the cloud base (*11*).

Further implications hinge on our corollary finding that extreme variations in boundary-layer aerosol concentrations, from polluted to clean conditions, influence anvil properties less than do mid-tropospheric aerosol concentrations (Fig. 2, E and F). Thus, the documented long-range transport of pollution in the middle and upper troposphere (*33*) may notably affect cirrus radiative properties, evolution, and lifetime. However, the details of such effects are not obvious. Recent surveys of aerosol number and size derived from multiple field experiments over tropical and subtropical regions demonstrate that there are often more than twice as many aerosols present in clean mid-tropospheric air at 6 to 10 km than in polluted air (*34*) and that the aerosol number at 8 to 12 km is highest when the atmosphere is devoid of nonvolatile pollution aerosols (*35*). Thus, pollution and aerosol number, which are closely correlated in the boundary layer, are frequently anticorrelated in the upper troposphere, perhaps owing to the scavenging of aerosol nucleation precursor gases by existing pollution aerosol surface area (*35*). It is thus possible that more polluted environments would yield fewer, larger anvil crystals than cleaner environments, in direct contrast to the aforementioned case of marine stratocumulus, wherein polluted environments yield more, smaller cloud particles. Because supersaturations may reach high values in cumulonimbus updrafts (*22*) and aerosol activation is therefore sensitive to cloud dynamics, a detailed analysis of aerosol size distributions and geographic variations in cloud dynamics is required to establish the overall effect of pollution on anvil cirrus clouds. Our analysis nonetheless indicates that long-range transport of pollution can dominate the effect of local sources on subtropical anvil clouds.

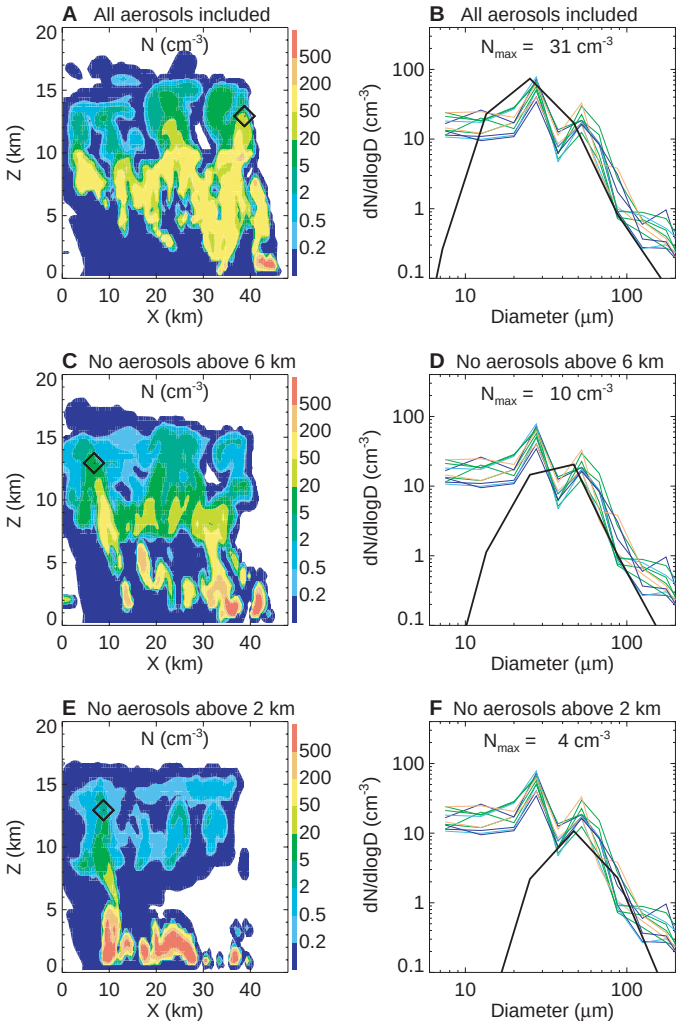

Fig. 4. A cross section (horizontal distance, *X*, versus elevation, *Z*) of simulated cloud particle number concentration, *N*, with a black diamond at the 13-km location of highest predicted number (**A**) and the ice crystal size distributions, *dN*/*dlogD* (**B**), simulated at that location (black line) and measured at 12 to 14 km on 21 July (colored lines). Simulated peak diameters closely match measured peak diameters at 20 to 30 μm when all aerosols are included [(A) and (B)] but shift to larger sizes, exhibiting successively poorer agreement with the measurements, when aerosols are excluded above 6 km (**C** and **D**) and above 2 km (**E** and **F**).

References and Notes

1. H. Graf, *Science* **303**, 1309 (2004).
2. S. Twomey, *Atmos. Environ.* **8**, 1251 (1974).
3. B. A. Albrecht, *Science* **245**, 1227 (1989).
4. Intergovernmental Panel on Climate Change, *Climate Change 2001: The Scientific Basis*, J. T. Houghton *et al*., Eds. (Cambridge Univ. Press, Cambridge, 2001).
5. G. L. Stephens, S.-C. Tsay, P. W. Stackhouse Jr., P. J. Flatau, *J. Atmos. Sci.* **47**, 1742 (1990).
6. V. Ramanathan, W. Collins, *Nature* **351**, 27 (1991).
7. U. Lohmann, E. Roeckner, *J. Geophys. Res.* **100**, 16305 (1995).
8. R. S. Lindzen, M.-D. Chou, A. Y. Hou, *Bull. Am. Meteorol. Soc.* **82**, 417 (2001).
9. A. D. Del Genio, W. Kovari, *J. Clim.* **15**, 2597 (2002).
10. B. A. Wielicki *et al*., *Science* **295**, 841 (2002).
11. A. P. Khain, D. Rosenfeld, A. Pokrovsky, *Geophys. Res. Lett.* **28**, 3887 (2001).
12. V. T. J. Phillips, T. W. Choularton, A. M. Blyth, J. Latham, *Q. J. R. Meteorol. Soc.* **128**, 951 (2002).
13. S. C. Sherwood, *J. Clim.* **15**, 1051 (2002).
14. M. O. Andreae *et al*., *Science* **303**, 1337 (2004).
15. R. A. Houze Jr., *Cloud Dynamics* (Academic Press, San Diego, CA, 1977).
16. Materials and methods are available as supporting material on *Science* Online.
17. D. E. Stevens, A. S. Ackerman, C. S. Bretherton, *J. Atmos. Sci.* **59**, 3285 (2002).
18. E. J. Jensen, L. Pfister, A. S. Ackerman, O. B. Toon, A. Tabazadeh, *J. Geophys. Res.* **106**, 17237 (2001).
19. A. S. Ackerman, O. B. Toon, D. E. Stevens, J. A. Coakley Jr., *Geophys. Res. Lett.* **30**, 10.1029/2002GL016634 (2003).

20. M. Xue, D.-H. Wang, J.-D. Gao, K. Brewster, K. K. Droegemeier, *Meteorol. Atmos. Phys.* **82**, 139 (2003).
21. H. R. Pruppacher, J. D. Klett, *Microphysics of Clouds and Precipitation* (Kluwer Academic Publishers, Dordrecht, Netherlands, 1997).
22. W. D. Hall, *J. Atmos. Sci.* **37**, 2486 (1980).
23. M. Z. Jacobson, R. P. Turco, E. J. Jensen, O. B. Toon, *Atmos. Environ.* **28A**, 1327 (1994).
24. R. List, N. R. Donaldson, R. E. Stewart, *J. Atmos. Sci.* **44**, 362 (1987).
25. H. P. Meyers, P. J. DeMott, W. R. Cotton, *J. Appl. Meteorol.* **31**, 708 (1992).
26. E. J. Zipser, in *Cloud Systems, Hurricanes, and the Tropical Rainfall Measuring Mission (TRMM)*, W.-K. Tao, R. Adler, Eds., vol. 29 of *Meteorological Monographs* (American Meteorological Society, Boston, MA, 2003), chap. 5.
27. R. S. Scorer, *Environmental Aerodynamics* (Wiley, New York, 1977).
28. D. J. Musil, A. J. Heymsfield, P. L. Smith, *J. Climate Appl. Meteorol.* **25**, 1037 (1986).
29. T. J. Garrett, H. Gerber, D. G. Baumgardner, C. H. Twohy, E. M. Weinstock, *Geophys. Res. Lett.* **30**, 10.1029/2003GL018153 (2003).
30. S. C. Sherwood, *Science* **295**, 1272 (2002).
31. P. K. Wang, *J. Geophys. Res.* **108**, 10.1029/2002JD002581 (2003).
32. R. G. Knollenberg, K. Kelly, J. C. Wilson, *J. Geophys. Res.* **98**, 8639 (1993).
33. J. Lelieveld *et al.*, *Science* **298**, 794 (2002).
34. A. D. Clarke, V. N. Kapustin, *J. Atmos. Sci.* **59**, 363 (2002).
35. H. B. Singh *et al.*, *J. Geophys. Res.* **107**, 10.1029/2001JD000486 (2002).
36. We thank J. Smith and B. Toon for raising questions about the relative importance of boundary-layer and free tropospheric aerosols, E. Zipser for sharing his experience with tropical convection, W. McKie for keeping our more than 70 computer processors running in concert from Key West to Mountain View, and D. Anderson for leading CRYSTAL-FACE with long-term vision. All of the data collection and modeling associated with this work was coordinated by NASA's Earth Science Enterprise through NRA-01-OES-02, with funding and support provided by NASA, NOAA, NSF, the U.S. Department of Energy (DOE), the Office of Naval Research, and the United States Weather Research Program. We gratefully acknowledge additional computing support provided by DOE's High Performance Computing Facility.

Supporting Online Material
www.sciencemag.org/cgi/content/full/304/5671/718/DC1
Materials and Methods
References

19 December 2003; accepted 24 March 2004

Missing OH Reactivity in a Forest: Evidence for Unknown Reactive Biogenic VOCs

Piero Di Carlo,[1,2]* William H. Brune,[1] Monica Martinez,[1]† Hartwig Harder,[1]† Robert Lesher,[1] Xinrong Ren,[1] Troy Thornberry,[3,4]‡ Mary Anne Carroll,[3,4] Valerie Young,[5] Paul B. Shepson,[6] Daniel Riemer,[7] Eric Apel,[8] Colleen Campbell[4]

Forest emissions of biogenic volatile organic compounds (BVOCs), such as isoprene and other terpenes, play a role in the production of tropospheric ozone and aerosols. In a northern Michigan forest, the direct measurement of total OH reactivity, which is the inverse of the OH lifetime, was significantly greater than expected. The difference between measured and expected OH reactivity, called the missing OH reactivity, increased with temperature, as did emission rates for terpenes and other BVOCs. These measurements are consistent with the hypothesis that unknown reactive BVOCs, perhaps terpenes, provide the missing OH reactivity.

Emissions of natural or biogenic volatile organic compounds (BVOCs) from vegetation are estimated to exceed all emissions of anthropogenic volatile organic compounds on the global scale and are roughly equal to global emissions of methane (*1*, *2*). They can have a dominant influence on the atmospheric chemistry of forests, rural areas, and some cities (*3*). The type of vegetation, solar radiation, and temperature determine the emission rates and species of BVOCs (*4*).

BVOCs react with hydroxyl radicals (OH) and nitrate radicals (NO_3), and olefinic BVOCs also react with ozone (O_3). A chemical's reaction frequency with OH is the product of its rate-coefficient for reaction with OH times its concentration. The sum of the reaction frequencies with OH for all chemicals is called the OH reactivity, which is the inverse of the OH lifetime. The calculated OH reactivity for the BVOCs that are emitted annually in North America has contributions from isoprene (51%), terpenes (31%), oxygenated BVOCs such as alcohols (16%), and all other known BVOCs (2%) (*4*). Oxidation of BVOCs by OH in the presence of nitric oxide (NO) is the principal source of tropospheric O_3 (*5*, *6*). At the same time, O_3 reacts with olefinic BVOCs, such as isoprene and terpenes, to produce OH (*7–9*). Oxidation of some BVOCs by OH, O_3, and NO_3 produces organic acids that have low vapor pressures and thus condense to form secondary organic aerosols (*10–14*). Understanding the OH reactivity is key to assessing the importance of these biogenic emissions to O_3 and aerosol formation.

Recent indirect evidence indicates that forests emit unknown, reactive BVOCs, perhaps terpenes (*12*, *15*, *16*). In a Michigan forest in 1998, Faloona *et al*. observed unexpected nocturnal OH, late-evening new particle formation, and a dependence of nocturnal OH and hydroperoxyl radicals (HO_2) on O_3 (*15*). In a Sierra Nevada forest in 2000 and 2001, significant chemical loss of O_3 was observed (*16*). Finally, in the boreal Hyytiälä forest (in Finland) in 2000, new particle formation of biogenic origin was observed; ancillary measurements suggest that the particles were produced from oxidation of terpenes (*12*). We show that forests emit reactive, unmeasured BVOCs with properties similar to those of terpenes.

This evidence comes from the direct measurement of OH reactivity. Measurements were made from 5 July to 3 August 2000, during the Program for Research on Oxidants: Photochemistry, Emissions and Transport (PROPHET 2000) intensive campaign. The site was at the University of Michigan Biological Station (45°30′N, 84°42′W) in the Great Lakes Region in northern Michigan (*17*). Measurements were made 2 m below the top of a 31-m tall tower, ~10 m above the canopy height. The site is in a mixed, transition forest that consists of northern hardwood, aspen, and white pine. During this period, the site experienced both clean Canadian air from the north and polluted air from cities to the south, such as Chicago and Detroit.

Direct atmospheric measurements of total OH reactivity were made with an instrument called the Total OH Loss-rate Measurement (TOHLM) (*18*, *19*). The TOHLM method is analogous to the discharge-flow technique used in laboratory kinetics studies (*20*, *21*). OH is generated at mixing ratios of a few parts per trillion by volume

[1]Department of Meteorology, Pennsylvania State University, University Park, PA 16802, USA. [2]CETEMPS–Dipartimento di Fisica, Università di L'Aquila, 67010 Coppito, L'Aquila, Italy. [3]Department of Atmospheric, Oceanic, and Space Sciences, [4]Department of Chemistry, University of Michigan, Ann Arbor, MI 48109, USA. [5]Department of Chemical Engineering, Ohio University, Athens, OH 45701, USA. [6]Department of Chemistry, Purdue University, West Lafayette, IN 47301, USA. [7]Rosenstiel School of Marine and Atmospheric Science, University of Miami, Miami, FL 33124, USA. [8]National Center for Atmospheric Research, Boulder, CO 80305, USA.

*To whom correspondence should be addressed. E-mail: piero.dicarlo@aquila.infn.it
†Present address: Max-Planck-Institut für Chemie, D-55128 Mainz, Germany.
‡Present address: National Oceanic and Atmospheric Administration, Aeronomy Lab, Boulder, CO, USA